Multifunctional Fullerene-Mediated Assembly of Gold Nanoparticles

I-Im S. Lim,[†] Jianying Ouyang,[‡] Jin Luo,[†] Lingyan Wang,[†] Shuiqin Zhou,[‡] and Chuan-Jian Zhong*[,†]

Department of Chemistry, State University of New York at Binghamton, Binghamton, New York 13902, and Department of Chemistry, College of Staten Island, and The Graduate Center, City University of New York, Staten Island, New York 10314

Received September 1, 2005
Revised Manuscript Received November 8, 2005

The assembly of nanoparticles using macromolecules as mediators into composite architectures provides opportunities for exploring the fine-tunable interparticle spatial and macromolecular properties in many areas of nanoparticle-structured technologies.[1] Some of the existing assembly strategies involved layer-by-layer,[2,3] DNA,[4] polymeric[5] recognition and mediator-templating[6−8] of molecularly capped nanoparticles. Fullerene (C_{60})-capped nanoparticles have recently begun to attract interests of materials research.[9−16] Examples include van der Waals interaction based assembly of un-functionalized C_{60} and Au nanoparticles,[9] covalent layer-by-layer assembly of C_{60}-capped nanoparticles,[10] and electrostatically linked C_{60} derivatives to CdTe nanoparticles.[11−12] However, the ability to assemble C_{60}-nanoparticles into 3D architectures with tunable interparticle chemistry has not been realized. We report herein a novel strategy to such ability by exploring the chemically tunable multifunctional interactions between negatively charged groups on gold nanoparticles (Au_{nm}) and positively charged piperazinyl groups on 1-(4-methyl)piperazinyl fullerene (MPF) (Scheme 1). In contrast to earlier work, the multifunctionalized fullerene is used to assemble citrate-capped gold nanoparticles in aqueous solution; and more importantly, it explores electrostatic interaction between the negatively charged nanoparticles and the positively charged fullerenes. In addition to the design of functional nanomaterials (e.g., controlled drug delivery and optical sensing), an important driving force for the fullerene−nanoparticle combination is to harvest the unique electron or energy transfer properties that cannot be obtained with individual gold nanoparticles or fullerenes. For example, the exploration of the photophysical properties in self-organization of porphyrin (donor) and fullerene (acceptor) units by clusterization with gold nanoparticles has recently been demonstrated for organic solar cells.[17] The self-assembly of gold nanoparticles as the central nanocore and appended fullerene moieties as the photoreceptive shell is also demonstrated for photoactive antenna system.[18] The exploration of these properties expands the well-documented photochemical properties of porphyrin−fullerene dyads.[19]

Scheme 1. Schematic Illustration of MPF-Mediated Assembly of Nanoparticles

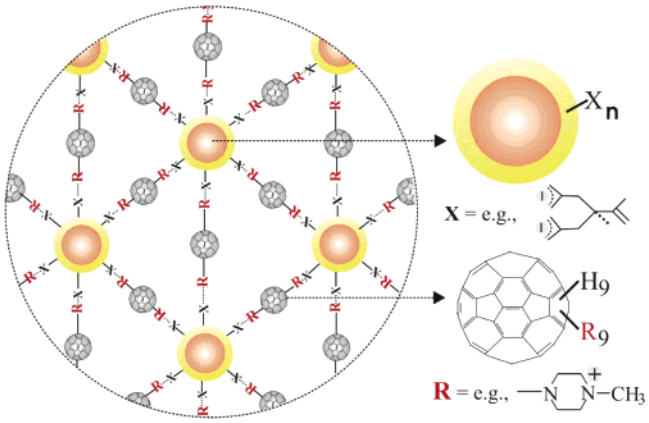

The number of piperazinyl groups on MPF is synthetically or chemically controllable, which we consider as an ideal building block for defining the interparticle spatial or chemical properties. The MPF synthesized[20] has an average stoichiometry of $[C_{60}H_9(NC_4H_8NCH_3)_9]$ as determined by X-ray photoelectron spectroscopy. Citrate-capped gold nanoparticles (Au_{nm})[21] have an average particle size of 11.5 ± 0.6 nm as determined by TEM. The stock concentration of Au_{nm} was determined based on molar absorptivity (ϵ_{Au} ~2.0 × 10^8 $M^{-1}\cdot cm^{-1}$) and the average particle size.[21] Stock solutions of MPF were prepared by dissolving MPF in H_2O (or with 1% DMSO) and filtered using 0.45-μm filters.

* To whom correspondence should be addressed. E-mail: cjzhong@binghamton.edu.
[†] State University of New York at Binghamton.
[‡] College of Staten Island and City University of New York.

(1) Templeton, A. C.; Wuelfing, W. P.; Murray, R. W. *Acc. Chem. Res.* **2000**, *33*, 27.
(2) Wuelfing, W. P.; Zamborini, F. P.; Templeton, A. C.; Wen, X. G.; Yoon, H.; Murray, R. W. *Chem. Mater.* **2001**, *13*, 87.
(3) Zamborini, F. P.; Hicks, J. F.; Murray, R. W. *J. Am. Chem. Soc.* **2000**, *122*, 4514.
(4) Mirkin, C. A.; Letsinger, R. L.; Mucic, R. C.; Storhoff, J. J. *Nature* **1996**, *382*, 607.
(5) Boal, A. K.; Ilhan, F.; DeRouchey, J. E.; Thurn-Albrecht, T.; Russell, T. P.; Rotello, V. M. *Nature* **2000**, *404*, 746.
(6) Maye, M. M.; Chun, S. C.; Han, L.; Rabinovich, D.; Zhong, C. J. *J. Am. Chem. Soc.* **2002**, *124*, 4958.
(7) Maye, M. M.; Lim, I.-I. S.; Luo, J.; Rab, Z.; Rabinovich, D.; Liu, T.; Zhong, C. J. *J. Am. Chem. Soc.* **2005**, *127*, 1519.
(8) Lim, I.-I. S.; Maye, M. M.; Luo, J.; Zhong, C. J. *J. Phys. Chem. B* **2005**, *109*, 2578.
(9) Brust, M.; Kiely, C. J.; Bethell, D.; Schiffrin, D. J. *J. Am. Chem. Soc.* **1998**, *120*, 12367.
(10) Shon, Y.-S.; Choo, H. *Chem. Commun.* **2002**, 2560.
(11) Guldi, D. M.; Zilbermann, I.; Anderson, G.; Kotov, N. A.; Tagmatarchis, N.; Prato, M. *J. Am. Chem.* Soc. **2004**, *126*, 14340.
(12) Guldi, D. M.; Zilbermann, I.; Anderson, G.; Kotov, N. A.; Tagmatarchis, N.; Prato, M. *J. Mater. Chem.* **2005**, *15*, 114.
(13) Shih, S.-M.; Su, W.-F.; Lin, Y.-J.; Wu, C.-S.; Chen, C.-D. *Langmuir* **2002**, *18*, 3332.
(14) Zhang, P.; Li, J.; Liu, D.; Qin, Y.; Guo, Z.-X.; Zhu, D. *Langmuir* **2004**, *20*, 1466.
(15) Guo, Z.-X.; Sun, N.; Li, J.; Dai, L.; Zhu, D. *Langmuir* **2002**, *18*, 9017.
(16) Deng, F.; Yang, Y.; Hwang, S.; Shon, Y.-S.; Chen, S. *Anal. Chem.* **2004**, *76*, 6102.
(17) Hasobe, T.; Imahori, H.; Kamat, P. V.; Ahn, T. K.; Kim, S. K.; Kim, D.; Fujimoto, A.; Hirakawa, T.; Fukuzumi, S. *J. Am. Chem. Soc.* **2005**, *127*, 1216.
(18) Sudeep, P. K.; Ipe, B. I.; Thomas, K. G.; George, M. V.; Barazzouk, S.; Hotchandani, S.; Kamat, P. V. *Nano Lett.* **2002**, *2*, 29.
(19) Schuster, D. I. *Carbon* **2000**, *38*, 1607.
(20) Goh, S. H.; Lee, S. Y.; Lu, Z. H.; Huan, C. H. A. *Macromol. Chem. Phys.* **2000**, *201*, 1037.
(21) Maye, M. M.; Han, L.; Kariuki, N. N.; Ly, N. K.; Chan, W.-B.; Luo, J.; Zhong, C. J. *Anal. Chim. Acta* **2003**, *496*, 17.

10.1021/cm051975r CCC: $30.25
Published on Web 11/25/2005

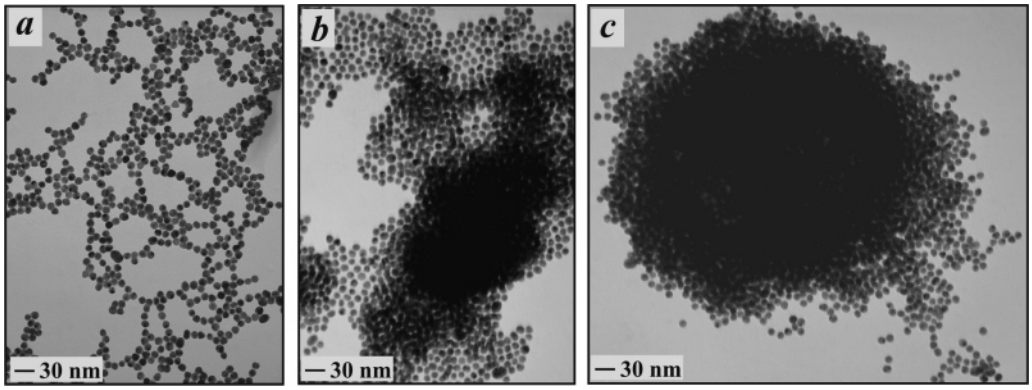

Figure 1. TEM images for Au_{nm} nanoparticles (a) and MPF−Au_{nm} assemblies obtained at $r \sim 4390$ (b) and ~ 7440 (c).

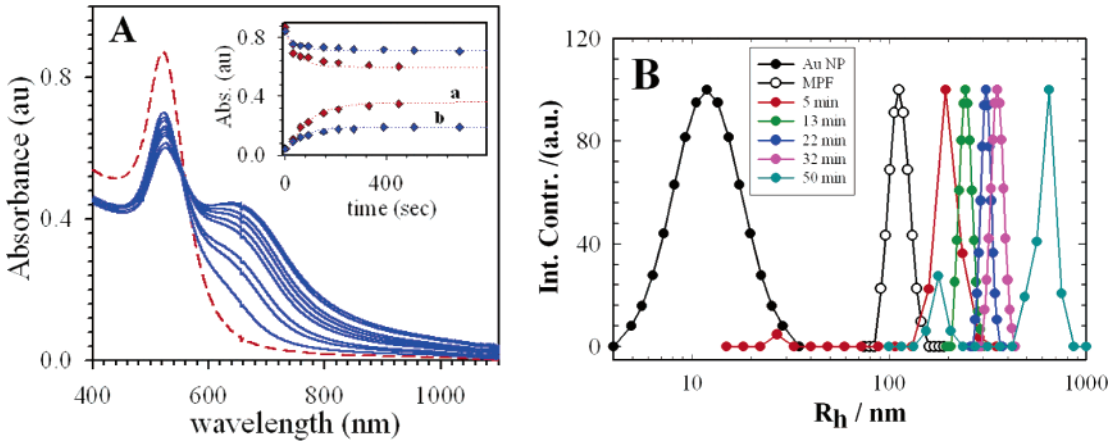

Figure 2. (A) UV−Vis for MPF−Au_{nm} assembly at $r \sim 4000$ (blue) (dashed line: Au_{nm}). Insert: kinetic plots for high (a, red) and low r (b, blue) for the increase of the Abs_{680nm} and decrease of Abs_{520nm}. (B) DLS: apparent hydrodynamic radius (R_h) distributions by intensity for MPF-mediated assembly of Au_{nm} (scattering angle: 30°). The main peaks for the curves of 5, 13, 22, 32, and 50 min correspond to right-most five curves at 201, 246, 311, 355, and 627 nm, respectively.

The MPF-mediated assemblies of Au_{nm} were sampled after adding MPF into an aqueous solution of Au_{nm} and were examined using TEM (Figure 1). In contrast to the relatively scattered 2D fractal morphology for Au_{nm} (a), the observation of highly clustered features with arrays or ensembles of Au_{nm} for the MPF-mediated assembly (b) indicates 3D interparticle linking. The MPF-to-Au_{nm} molar ratio (r = [MPF]:[Au_{nm}] ~ 1) translates to ~0.01 piperazinyl groups anchored on fullerene per citrate group capped on Au_{nm} (MPF has 9 piperazinyl groups whereas the 11.5-nm particle can accommodate ~1250 citrates), implying that there are more than sufficient citrate molecules available for interacting with the piperazinyl groups. Because the negative charges are 2 orders of magnitude higher than the positive charges on MPF, it is not a simple surface neutralization effect that is responsible for the interparticle assembly.

The size of the assembly was found to increase with the MPF-to-Au_{nm} molar ratio and assembling time. For $r = 7440$ (c), the resulting highly clustered 3D ensemble of Au_{nm} exhibits a large spherical shape. The less-well defined edge is likely due to the drying effect of water from the aqueous environment, in contrast to the well-defined spherical edges found for assemblies in organic environment (e.g., multidentate thioether-mediated assembly of nanoparticles in toluene).[6−7] If the assembly were due to simple surface neutralization, fused nanoparticles would have been formed because of the disruption of surface protection. In fact, separate experiments using other positively charged molecules (e.g., tetramethylammounim) did not show any assembly even at much higher concentrations, further ruling out the possibility of a simple surface neutralization effect.

The fact that there were hardly any free nanoparticles or fractal morphologies being spotted for the MPF−Au_{nm} samples (b−c) was indicative of the interparticle linkages of particles by the multifunctional MPF, which was substantiated by the analysis of the interparticle distance. The edge-to-edge interparticle distance determined from the interconnected Au_{nm} particles in the TEM image (a) yielded an average value of 1.14 ± 0.20 nm. For interparticle linking via two surface-adsorbed citrate molecules, a theoretical estimate of the edge-to-edge interparticle distance would be 1.28 nm, which could be slightly overestimated in view of the likelihood of interdigitated shell interactions. It is quite close to the observed interparticle distance. In contrast, the measured interparticle distance for MPF−Au_{nm} assemblies (b) displays a larger value, 2.52 ± 0.27 nm. Considering that the piperazinyl group on MPF is protonated at the nitrogen next to methyl group, a theoretical estimate of the edge-to-edge interparticle distance for the MPF−Au_{nm} assembly yields a value of 3.19 nm. This value is slightly larger than the measured one, likely implying a certain degree of inter-penetration between the protonated piperazinyl groups and the carboxylate shells.

The nanoparticle solution showed a gradual color change from red to purple as a result of the assembly. In contrast to the appearance of surface plasmon (SP) resonance band at

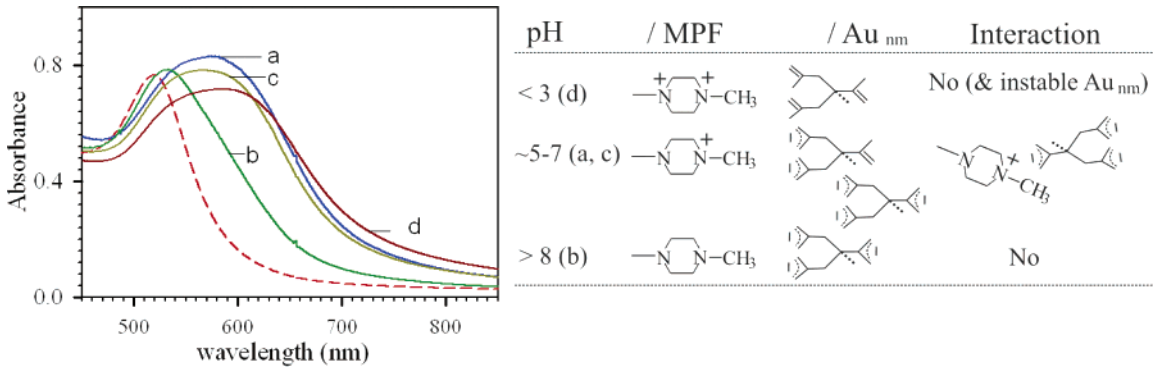

Figure 3. pH-tuning of MPF−Au_{nm} assembly and disassembly. UV−Vis spectra for Au_{nm} (dashed line), MPF−Au_{nm} assembly at pH 5 (a); upon changing pH to 10 (b); upon changing pH to 7 (c); and upon changing pH to 2 (d). Each curve was taken after 30 min. Chart: pH-dependent electrostatic interactions between piperazinyl and citrate groups.

520 nm for Au_{nm},[21] a new SP band for MPF−Au_{nm} assemblies in the aqueous solution was found at ~680 nm (Figure 2A). The spectral evolution is indicative of the change in interparticle distance and dielectric medium properties.[6,7] The molar ratio has a significant effect on the spectral evolution. At r ~4000 (pH 5), the increase of absorbance for the new band at ~680 nm was accompanied by a decrease of the 520 nm band. The reactivity is evidenced by the kinetics of the absorbance data for r ~4000 (a) and ~2000 (b) (insert). Both showed an exponential rise for the 680 nm band and decrease for the 520 nm band, with a clear difference in reaction rate. At the lower r, the purplish color of the solution remained for 2 days before precipitation, whereas precipitation occurred within a day for the higher r. The precipitated assemblies were redispersable by brief sonication. Importantly, the distinct isosbestic point observed around ~580 nm indicates the presence of two light-absorbing species at equilibrium (i.e., Au_{nm} and MPF−Au_{nm} assemblies).

The dynamic light scattering (DLS) data for the assembly of MPF−Au_{nm} (Figure 2B) evidenced the change of the apparent hydrodynamic radius (R_h) corresponding to the above spectral evolution. It is evident that the size of the assemblies grew with reaction time, up to ~700 nm. The R_h distributions are based on scattered intensity contribution. In the case of large assemblies with R_h ~ 200 nm, the detection of the small peak with R_h ~ 28 nm could be attributed to the early stage of the assembly. The small-sized assemblies were dominant at the early stage of assembling. After ~10 min, only highly monodispersed assemblies with R_h ~246 nm were observed. The size of the monodispersed MPF-mediated assemblies was observed to continuously grow with reaction time till the occurrence of phase separation (~40 min). The findings support that the size of the MPF−Au_{nm} assembly is controllable.

The interparticle interaction for the MPF−Au_{nm} assembly was also found to be tunable by pH. On the basis of pK_a values for citric acid (pK_a = 3.1(a_1), 4.8(a_2), and 6.4(a_3)[22a]) and piperazine (pK_a = 4.2(a_1) and 8.4(a_2)[22b]) groups, the electrostatic interaction involved at least two of the deprotonated $-CO_2H$ groups in citrate and one protonated piperazinyl ($-NC_4H_8N^+HCH_3$) of C_{60} at pH ~5. Indeed, when pH is increased to above 8, no apparent spectral evolution was observed. The control of pH was found to tune the

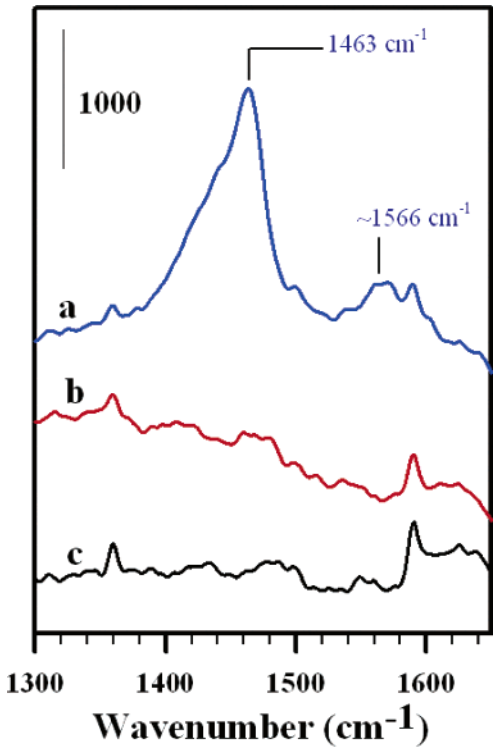

Figure 4. SERS spectra for a solution sample of MPF−Au_{nm} assembly ([Au_{nm}] = 0.75 nM; [MPF] = 6.9 μM) (a). Spectra for solution samples of Au_{nm} (b) and MPF (c) under identical concentrations are included for comparison. (Integration time = 50 s.)

assembly and disassembly processes effectively (Figure 3). Upon increasing pH from ~5 (a) to 10 (b), the SP band shifted from ~580 nm to the wavelength (b) approaching the SP band for Au_{nm}, indicating the disassembly of MPF−Au_{nm} into individually isolated Au_{nm} particles. This assessment was indeed evidenced by the lack of any nanoparticle-clustering feature in the TEM data. As illustrated by the chart in Figure 3, the pH-tuned disassembly is due to the absence of electrostatic interactions between MPF and Au_{nm} because MPF is neutral whereas citrate is negatively charged. This process was reversible because the SP band shifted back upon decreasing pH to ~7 (c). At pH ~2 (d), irreversible precipitation and long-wavelength broadening of the SP band

(22) (a) Dean, J. A. *Lange's Handbook of Chemistry*; McGraw-Hill: New York, 1972. (b) Santos, M. A.; Esteves, M. A.; Vaz, M. C.; Frausto da Silva, J. J. R.; Noszal, B.; Farkas, E. *J. Chem. Soc., Perkin Trans.* **1997**, *2*, 1977.

were observed as a result of instability of the citrate capping on Au_{nm} at low pH, which was supported by TEM observation of larger aggregates in which individual nanoparticles could hardly be identified. We have performed control experiments which showed that the pH-tuned changes in color or precipitation were different with and without the fullerene mediator, demonstrating the importance of the interparticle molecular interaction, which would be pH-independent if there were no binding of MPF to gold particles by the electrostatic interaction. The pH-tuned change in optical properties has implications to controlled release of molecules from the nanoparticle assembly, an area of importance in controlled drug release.

Surface enhanced Raman spectroscopy (SERS) is a powerful tool to probe the adsorption of macromolecules on the surface of noble metals. Figure 4 presents a representative SERS spectrum for an aqueous solution of Au_{nm} in which MPF was added to ensure a full monolayer of coverage on the gold surface. In contrast to the practically background-like spectra for solution samples of Au_{nm} (b) and MPF (c) with concentrations identical to the solution of MPF−Au_{nm} (a), two clear bands are observed at 1463 and 1566 cm^{-1} for MPF−Au_{nm} (a). These two bands can be assigned to A_g-(2) mode (1470 cm^{-1}) and H_g(8) mode (1575 cm^{-1}) for the Raman-active vibration modes of C_{60}.[23,24] The detection of SERS for these two bands is clearly due to the surface effect of gold nanoparticles, a strong piece of evidence supporting the adsorption of MPF on the surface of gold nanoparticles, which is responsible for the MPF−Au_{nm} assembly. The SERS effect could not be detected without this binding. An important implication of the finding is that the MPF−Au_{nm} combination provides an effective spectroscopic probe for the high-sensitivity detection as a result of the SERS effect.

We have demonstrated the multifunctional fullerene-mediated assembly of metal nanoparticles into 3D architectures and the optical tunability in the controllable assembly and disassembly processes. The SERS result provided evidence for the surface binding and further demonstrated the benefit of the fullerene−nanoparticle combination over the individual components. With further correlation between the optical or spectroscopic properties and the nanoscale morphologies, the findings are expected to provide new design parameters of novel nanostructures for potential applications such as controlled drug-delivery, optical sensors and spectroscopic probes.

Acknowledgment. This work is supported by the National Science Foundation (CHE 0349040 (for work at SUNY) and CHE 0316078 (for work at CUNY)). I-I.S.L. acknowledges the support of the National Science Foundation Graduate Research Fellowship.

Note Added after ASAP Publication. There was an error in the approximate value of *r* in the version published ASAP November 25, 2005; the corrected version was published December 14, 2005.

CM051975R

(23) Chase, S. J.; Bacsa, W. S.; Mitch, M. G.; Pilione, L. J.; Lannin, J. S. *Phys. Rev. B* **1992**, *46*, 7873.
(24) Menéndez, J.; Page, J. B. Vibrational spectroscopy of C_{60}. In *Light Scattering in Solids VIII*; Cardona, M., Güntherodt, G., Eds.; Springer: Berlin, 2000.